

**A study of contact binaries with large temperature differences  
between components<sup>†</sup>**Michał Siwak<sup>1,2</sup>, Stanisław Zola<sup>1,3</sup>, Dorota Koziel-Wierzbowska<sup>1</sup><sup>1</sup> Astronomical Observatory of the Jagiellonian University, ul. Orla 171, 30-244 Kraków,  
e-mail: siwak@oa.uj.edu.pl,<sup>2</sup> Department of Astronomy and Astrophysics, University of Toronto, 50 St. George Street,  
M5S 3H4 Toronto, Ontario,  
e-mail: siwak@astro.utoronto.ca,<sup>3</sup> Mount Suhora Astronomical Observatory, Cracow Pedagogical University,  
ul. Pochorążych 2, 30-084 Kraków*Received 25 11, 2010*

## ABSTRACT

We present an extensive analysis of new light and radial-velocity (RV) curves, as well as high-quality broadening-function (BF) profiles of twelve binary systems for which a contact configuration with large temperature differences between components has been reported in the literature. We find that six systems (V1010 Oph, WZ Cyg, VV Cet, DO Cas, FS Lup, V747 Cen) have near-contact configurations. For the remaining systems (CX Vir, FT Lup, BV Eri, FO Hya, CN And, BX And), our solutions of the new observations once again converge in a contact configuration with large temperature differences between the components. However, the bright regions discovered in the BFs for V747 Cen, CX Vir, FT Lup, BV Eri, FO Hya, and CN And, and further attributed to hot spots, shed new light on the physical processes taking place between the components and imply the possibility that the contact configurations obtained from light- and RV-curve modelling are a spurious result.

**Key words:** *eclipsing binaries, contact binaries, physical parameters: individual: V1010 Oph, WZ Cyg, VV Cet, DO Cas, FS Lup, V747 Cen, CX Vir, FT Lup, BV Eri, FO Hya, CN And, BX And*

**1. Introduction**

Theoretical investigation of W UMa-type binary stars began with the work of Kuiper (1941), who found that contact binary stars with components belonging to

---

<sup>†</sup>Based on observations obtained at:

- the *Fort Skala* Astronomical Observatory of the Jagiellonian University;
- the Mount Suhora Astronomical Observatory, Cracow Pedagogical University;
- the David Dunlap Observatory, University of Toronto;
- the South African Astronomical Observatory, with the 1.9, 0.75, and 0.5 m telescopes;
- the ESO-La Silla Observatory with the 2.2 m telescope, under programme ID 077.D-0789;
- the Las Campanas Observatory, Carnegie Institute of Washington with the 2.5 m Du Pont telescope.

the Main Sequence (MS) cannot exist in an equilibrium state (a result known as the *Kuiper paradox*). Lucy (1968) has shown that Kuiper's conclusion is valid only for contact binary stars with radiative common envelopes and unequal-mass components: contact binaries consisting of MS stars with common convective envelopes can exist in hydrodynamical and thermal equilibrium states if CNO and p-p cycles occur in the cores of both components. According to Lucy's common-envelope model, both stars in a contact binary system should have equal effective temperatures. Although this result resolved the Kuiper paradox, Lucy's theoretical models of contact binary stars with components differing in their structure because of CNO and p-p cycle reactions covered only the blue end of the period-color diagram (Eggen, 1967).

The small masses of primary components obtained from combined radial-velocity (RV) and light-curve modelling (Lucy, 1973) prompted Lucy (1976) and Flannery (1976) to consider a situation with both solar-type components harbouring p-p reactions. It turned out that in such a situation it is not possible to attain a thermally stable equilibrium. Instead, in a thermal time scale of 10 million years, systems will oscillate between contact and semi-detached configurations. Robertson & Eggleton (1977) performed more realistic computations, taking into account an angular-momentum loss during a system evolution. As a result, they obtained models of contact-binary systems with physical parameters of components closely resembling those obtained from light- and RV-curve modelling.

According to the leading work on the Thermal Relaxation Oscillation (TRO) theory (Lucy, 1976; Flannery 1976), the maximum temperature difference ( $\Delta T$ ) between components of solar-type contact-binary system should not exceed 880–1000 K. Similar values have been recently obtained by Li et al. (2004a, 2004b, 2005) and Kähler (2004). The marginal-contact configurations and temperature differences between the components in the 300–700 K range obtained for RW PsA, AK Her, and W Crv by Lucy & Wilson (1979) have confirmed the theoretical findings.

Kałużny (1983, 1985, 1986), Hilditch et al. (1984), and Hilditch & King (1988) have found other contact systems exhibiting large  $\Delta T$  between their components. For some of these systems, light-curve modelling resulted in temperature differences that were considerably larger than the theoretical limit of about 1000 K. Rucinski (1986) and Eggleton (1996) proposed that indications of contact binaries with such large temperature differences are in fact artefacts caused by the application of simple Roche lobe-based light curve synthetic models, with disregard for intensive accretion processes expected to take place between components during short and violent phases when a contact configuration is broken or re-established.

In Table 1, we present a sample of close binary stars for which at least one light-curve solution was previously obtained using a light-curve synthesis program based on the Roche model and yielded a contact configuration with a temperature difference between the components larger than 1000 K. However, as indicated in

column 7 of Table 1, almost all the models are based on photometric mass ratios, a limitation which significantly decreases the reliability of the obtained configurations. Closer inspection reveals that in many cases an O’Connell effect (i.e., occurrence of unequal maxima, most probably due to a combination of effects introduced by spots on one or both components) has not been taken into account during the light-curve modelling. Additionally, closer inspection reveals the applied albedo and gravity-darkening coefficients to have been far from their theoretical values. Moreover, the scatter visible in the light curves was often too large to permit a unique solution. We refer an interested reader to references given in the last column of Table 1 for more historical information about the targets investigated in this paper.

All the above has led us to the conclusion that in order to get unique configurations for these systems, one must obtain high quality light and RV curves (Section 2) and must perform advanced modelling on this data (Section 3). Results obtained from the modelling of individual systems are described in Sections 4 and 5. Physical parameters of these systems are presented in Section 6. In Sections 4 and 5 we also present a discovery of bright regions (hot spots) on secondary components, made possible by the outstanding quality of the broadening functions (BFs) obtained for some systems. In Section 7, we discuss the implications of this discovery for results obtained classically (i.e., obtained from light- and RV-curve fits within the Roche-lobe model).

## 2. Observations and data reduction

### 2.1. Spectroscopy

Medium-resolution spectra of FS Lup were obtained at the South African Astronomical Observatory (SAAO) in the second half of April 2006, with the 1.9 m Radcliffe telescope equipped with a slit spectrograph and the grating “no.4” (1200 l/mm). With the 1.2 arcsec-wide slit projected on 2.2 pixels of a CCD camera, this results in effective resolving power  $R = 8000$ . The star was observed in two spectral regions: during the first night the spectral window was centered at 4400Å, and during all other nights at 5250Å.

FT Lup, CX Vir, and V747 Cen were observed in service mode at ESO-La Silla during six nights of April, May, and June 2006. In this facility the 2.2 m MPG telescope equipped with the FEROS spectrograph provided high resolution ( $R = 48000$ ) and very good signal-to-noise spectra.

The targets reachable from the northern hemisphere (WZ Cyg, VV Cet, BX And, DO Cas, and BV Eri) were observed at the David Dunlap Observatory (DDO), a suburban facility then owned by the University of Toronto, during November and December of 2006 and February of 2007, with the DDO 1.9 m telescope and a slit spectrograph. Most of the data were obtained with the 2160 l/mm grating, but because of the relatively faint magnitude of VV Cet and WZ Cyg, during nights

Table 1

The sample of contact binary systems with large temperature differences between the components.

System	$T_{\text{eff}}^{\text{prim}}$ [K]	$T_{\text{eff}}^{\text{sec}}$ [K]	$\Delta T$ [K]	f(%)	conf.	q	First author, year
GW Tau	8750	5620	3130	11	C	0.309	Zhu+, 2006
V747 Cen	8500	4700	3800	4.3	m-c	0.399	Leung, 1974
	8260	4640			n-c	0.319	Barone+, 1991
DO Cas	7700	3850	3850	13	C	0.310	Kałużny, 1985
	7700	4000			SD1	0.325	Kałużny, 1985
	8500	4090			SD1	0.415	Karimie+, 1985
	9070	4830	4240	13	C	0.313	Oh+, 1992
	8300	4690			SD1	0.326	Barone+, 1992
V1010 Oph	8200	5670	2530	18	C	0.489	Leung+, 1977
	7500	5200			SD1	0.446	Corcoran+, 1991
	8200	5700			SD1	0.448	Niarchos+, 2003
VV Cet	8100	5900	2200	16	C	0.249	Rahman, 2000
BL And	7500	5370	2130	49	C	0.311	Kałużny, 1985
	7500	4830			SD1	0.377	Zhu+, 2006
WZ Cyg	7050	5750	1300	?	C	0.540	Rovithis+, 1999
FO Hya	6950	4260	2690	7	m-c	0.552	Candy+, 1997
BV Eri	6850	5650	1200	20	C	0.252	Gu, 1999
FT Lup	7400	5100	2300	?	C	0.400	Mauder+, 1982
	6700	4560	2140	?	C	0.430*	Hilditch+, 1984
	6700	4800	1900	12	C	0.430*	Kałużny, 1986
	6700	3920			SD1	0.465	Lipari+, 1986
BX And	6500	4680	1820	6	m-c	0.623	Samec+, 1989
	6800	4500	2300	8	m-c	0.497*	Bell+, 1990
CX Vir	6500	4500	2000	0	m-c	0.340*	Hilditch+, 1988
CN And	6500	5500	1000	?	m-c	?	Kałużny, 1983
	6200	4680	1520	43	C	0.579	Rafert, 1985
	6500	5920			SD1	0.389*	Van Hamme+, 2001
	6450	5375			SD2	0.371*	Zola+, 2005
	6160	4660	1500	17	C	0.390*	Jassur+, 2006
FS Lup	6000	4700	1300	33	C	0.510	Milano+, 1987

The line in the middle separates systems with radiative envelopes (above) from systems with convective envelopes (below). The column denoted “conf.” gives the configuration derived for the system in question: C for contact; m-c for marginal contact; SD1 and SD2 for semi-detached systems, where it is, respectively, the 1st or the 2nd component that fills its Roche lobe; and n-c for near-contact. The quantity  $f$  is the *fill-out* parameter, given only for contact and marginal-contact systems in cases in which we had the necessary data to make a computation through the equation  $f = (\Omega - \Omega_{L_1}) / (\Omega_{L_1} - \Omega_{L_2})$  (where  $\Omega_{L_1}$  and  $\Omega_{L_2}$  are the Roche potentials at the  $L_1$  and  $L_2$  points, respectively,  $\Omega$  being a common surface potential obtained from the light-curve modelling). We also show the mass ratios  $q$  obtained from the light-curve solution, adding an asterisk to mark cases in which a spectroscopic mass ratio was used.

of poor seeing (a few arcsec), the observations were made with a lower-resolution (1200 l/mm) grating. With the 1.5-arcsec slit projected on 2.5 pixels, the effective resolving power was  $R = 19000$  and  $R = 11000$  for the 2160 l/mm and 1200 l/mm

gratings, respectively.

FO Hya was observed at the Las Campanas Observatory (LCO) in February 2009 with the 2.5 m Du Pont telescope, equipped with the classical slit echelle spectrograph. With the 1-arcsec slit, this instrument assured spectral resolution of  $R = 40000$ .

The data gathered at the ESO-La Silla observatory were reduced in the usual way with FEROS-DRS under ESO-MIDAS. The data obtained at SAAO, DDO, and LCO were reduced with IRAF.

For RV measurements, we applied the BF method (Rucinski, 1992, 1999, 2002, and Pribulla et al., 2009; the 2009 publication has the fullest list of references). BFs were calculated on the basis of RV standards from the list of Stefanik et al. (1999), observed in all the observatories on the same nights as the main targets, and on the basis of synthetic spectra from the SPECTRUM software (Gray, 2001), using Kurucz's (1993) atmosphere models for MS stars with solar abundances.

RVs of light centroids were measured by means of synthetic rotational profiles for spherical stars. This choice assured reasonable model-independence, while still approximating very accurately the observed profiles of elliptically disturbed stars. As primary and secondary components of our targets have very different spectral types, the RVs of primary components were obtained from BF profiles calculated using the early-type RV standards, while RVs of secondary components were obtained from BF profiles calculated using late-type RV standards (Table 2). We found that in most cases this approach minimized scatter of RV curves and yielded almost identical (within  $1 - 2 \text{ km/s}$ ) mean system velocities  $v_\gamma$  for the primary and secondary components. The BF method gave larger semi-amplitudes of the RV variations ( $K_i$ ) than did the cross-correlation function (CCF) method previously applied for RV measurements of CX Vir (Hilditch & King, 1988), FT Lup (Hilditch et al., 1984) and BX And (Bell et al., 1990), thereby fully confirming the predictions of Rucinski (1999) that there would be a tendency for systematic reduction of  $K_i$  under the CCF approach.

Table 3 contains preliminary orbital parameters obtained from the new RV curves by fitting the sine-curve to the data in the phase ranges 0.15–0.35 and 0.65–0.85.

## 2.2. Photometry

New high-quality photometric data for targets reachable from the northern hemisphere were taken during the three consecutive northern autumn-winter seasons 2004/2005, 2005/2006, and 2006/2007. Most of the data were obtained with the Carl-Zeiss 50 cm telescope at the Fort Skała Astronomical Observatory of the Jagiellonian University. This telescope was equipped with the Photometrics S300 CCD camera with the SITe SI003B, 1024x1024 pixels chip, carrying a set of broad-band BVRI (Bessell) filters. With a focal length of 6.7 m, the field of view was 12 arcmin x 12 arcmin. In this observatory, we took complete light curves for

Table 2

Spectral regions and RV-standard stars used for the RV determination.

system	used spectral range [Å]	RV standards
FS Lup	3920-4750 & 4880-5640	HD 102870 (F8V) & HD 92588 (K1IV)
FT Lup	4378-5743 ( $H_{\beta}$ excluded)	F2V & K3V
CX Vir	4378-5743 ( $H_{\beta}$ excluded)	F5V & K0V + K3V
V747 Cen	4905-5743	A5V & K1V
FO Hya	4910-5560	F0V & K0V
V1010 Oph	5074-5305	HD 128167 (F2V) & HD 144571(G8V)
BV Eri	5074-5305	HD 128167 (F2V) & HD 65588 (G8V)
BX And	5074-5305	HD 128167 (F2V) & HD 3765 (K2V)
DO Cas	5074-5305	A5V & K1V
VV Cet	5074-5305	HD 222738 (F7V)
WZ Cyg	5074-5305	HD 222738 (F7V) & HD 3765 (K2V)

Table 3

Preliminary orbital parameters obtained by sine-curve fitting to spectroscopic observations in the phase ranges: 0.15-0.35 and 0.65-0.85.

system	$K_1$ [km/s]	$K_2$ [km/s]	$v_{\gamma}$ [km/s]	q
FO Hya	$62.48 \pm 0.97$	$253.20 \pm 4.50$	$55.80 \pm 0.90$	$0.247 \pm 0.009$
FS Lup	$112.10 \pm 0.87$	$236.36 \pm 3.05$	$12.74 \pm 0.84$	$0.474 \pm 0.010$
FT Lup	$112.21 \pm 0.37$	$239.22 \pm 3.28$	$-2.22 \pm 0.35$	$0.469 \pm 0.008$
CX Vir	$75.64 \pm 0.45$	$218.19 \pm 1.63$	$-11.47 \pm 0.42$	$0.347 \pm 0.005$
V747 Cen	$78.30 \pm 0.52$	$231.39 \pm 3.42$	$-18.57 \pm 0.49$	$0.338 \pm 0.007$
V1010 Oph	$107.32 \pm 0.46$	$226.32 \pm 0.85$	$-19.09 \pm 0.44$	$0.474 \pm 0.004$
BV Eri	$67.41 \pm 0.48$	$250.81 \pm 0.87$	$-39.89 \pm 0.48$	$0.269 \pm 0.003$
BX And	$106.35 \pm 0.61$	$233.58 \pm 1.77$	$-24.69 \pm 0.90$	$0.455 \pm 0.006$
DO Cas	$78.85 \pm 0.75$	$259.01 \pm 2.78$	$26.22 \pm 0.25$	$0.304 \pm 0.006$
VV Cet	$62.49 \pm 1.51$	$220.23 \pm 6.31$	$-0.01 \pm 1.42$	$0.284 \pm 0.015$
WZ Cyg	$130.91 \pm 1.05$	$205.11 \pm 3.54$	$0.98 \pm 1.52$	$0.638 \pm 0.016$

WZ Cyg, BX And, GW Tau, and BL And.

DO Cas, VV Cet, and CN And were observed at the Mount Suhora Observatory of the Cracow Pedagogical University using the Carl-Zeiss 60 cm telescope. The first two stars were observed with a three-channel photometer equipped with the Hamamatsu R2949 photomultipliers and broadband Johnson BVRI filters. CN And was observed using the SBIG ST10XME CCD camera (containing the KODAK KAF-3200E/ME chip) and wideband BVRI (Bessell) filters.

CX Vir and FT Lup were observed in April 2005 at the SAAO with the 50 cm Boller & Chivens telescope and a single-channel modular photometer equipped

with the Hamamatsu R943-02 GaAs photomultiplier and BV ( $RI$ )<sub>c</sub> Johnson-Cousins filters. In March 2006, at the same observatory, we observed V747 Cen with the 75 cm Grubb-Parsons telescope, equipped with the UCT CCD camera with the EEV 576x420 pixel chip (binned 2x2) and Johnson BVRI filters. The same telescope, but equipped with the single-channel UCT Photometer with the Hamamatsu RCA 31034A GaAs photomultiplier and Johnson-Cousins BV ( $RI$ )<sub>c</sub> filters, was used during April and May 2006 for observations of FS Lup and FO Hya.

Data gathered taken with CCD cameras were reduced in the standard way through ESO-MIDAS scripts. Aperture photometry with variable aperture size was performed through Kopacki's programs (private communication), based on the DAOPHOT II package (Stetson, 1987). Data obtained with single-channel photometers were dead-time corrected using the procedure given in the XLUCY manual (Balona, 2000). Sky-background and comparison star interpolations were applied with our own software. The data taken with the three-channel photometer at the Mount Suhora Observatory were reduced using dedicated computer programs developed by M. Drózdź (private communication). Standard corrections for differential extinction and colour extinction were applied to the new light curves.

Light and RV curves were phased with the most up-to-date elements determined by Kreiner (2005–2008, private communication). These ephemerides were obtained using the minima times included already in the Kreiner (2004) database, but supplemented with several new times of minima determined from our own observations. The comparison and check stars, as well as elements applied for phases calculation, are listed in Table 4.

As attempts to take RV curves of GW Tau and BL And failed in bad weather, these targets were excluded from the current investigation.

T a b l e 4

Comparison and check stars applied for differential photometry. The two right panels contain elements used for phases calculation.

system	comparison star(s)	check star(s)	$M_0$ [HJD]	$P$ [d]
BX And	mean of 3 stars	internal comp.	2453350.23061	0.61011240
WZ Cyg	mean of 3 stars	internal comp.	2454019.26728	0.58446762
VV Cet	GSC 4674 0662	no check star	2453675.39228	0.52239410
CN And	GSC 2787 1803	GSC 2787 1891	2452500.12040	0.46279081
FO Hya	GSC 6049 0074	no check star	2453855.35760	0.46955663
CX Vir	GSC 6137 0576	GSC 6138 0644	2453470.50082	0.74608003
FT Lup	GSC 7828 1478	GSC 7829 0247	2453478.64697	0.47008002
FS Lup	GSC 8292 1678	GSC 8292 0914	2452500.08800	0.38139970
V747 Cen	GSC 8261 1863	GSC 8261 0719	2453811.34417	0.53719482

### 3. Light- and RV-curve modelling: the method

Light- and RV-curve modelling was performed through the Wilson-Devinney (WD) code (Wilson, 1996), with a Monte Carlo search method applied to locate a global minimum in parameter space (Zola et al., 2010). An iterative procedure of light- and RV-curve modelling, introduced by Baran et al. (2004), was used during our computations. Errors of adjusted parameters were calculated from the search matrix at confidence level of 90%, as described by Kreiner et al. (2003). The values of a reduced (weighted)  $\chi^2$  were used to determine the quality of the obtained fits.

The effective-temperature-versus-spectral-type calibration of Harmanec (1988) was used to determine the effective temperatures of the primary components ( $T_{\text{eff}}^{\text{prim}}$ ) according to their spectral types. (Table 5 gives details.) This parameter, like the spectroscopic mass ratio  $q_{\text{spec}}$ , was not adjusted during light curve modelling. The albedo  $A$  and gravity-darkening coefficients  $g$  of both stars were assumed at the theoretical values, i.e.  $A = 1$ ,  $g = 1$  for stars with radiative envelopes ( $T_{\text{eff}} > 7200$  K) (von Ziepel, 1924), and  $A = 0.5$ ,  $g = 0.32$  for stars with convective envelopes ( $T_{\text{eff}} < 7200$  K) (Lucy 1967, Rucinski 1969). The square-root limb darkening law and the coefficients published by Díaz-Cordoves et al. (1995) and Claret et al. (1995) were assumed as a function of an effective temperature of a star and the effective wavelength of the filter. As the choice between the detailed and simple reflection-effect treatment turned out to have no practical impact on the obtained results, especially on the obtained configurations, we fitted our data under the assumption of a simple reflection model ( $mref = 1$ ) with a single reflection ( $nref = 1$ ).

During light curve modelling, we adjusted the orbital inclination  $i$ , the secondary-component effective temperature  $T_{\text{eff}}^{\text{sec}}$ , the Roche potentials  $\Omega$  and the luminosities  $L$  of both components, the phase shift, and the third light  $l_3$ . Additionally, if an O'Connell effect was visible in the light curves, we adjusted the spot parameters: its coordinates  $(\phi, \lambda)$ , a spot radius  $r$ , and the ratio between the spot temperature and the surrounding surface. During the RV-curve modelling, we adjusted the orbital semi-major axis  $a$ , the spectroscopic mass ratio  $q_{\text{spec}}$ , and the mean system velocity  $v_\gamma$ .

As the result of the iterative procedure of light- and RV-curve modelling, we obtained two groups of solutions. The first one comprises the evidently near-contact systems (V1010 Oph, WZ Cyg, VV Cet, DO Cas, FS Lup, and V747 Cen). The second comprises the systems whose light curves were better fitted by a contact configuration model, again with large temperature differences between the components (CX Vir, FT Lup, BV Eri, FO Hya, CN And, and BX And).



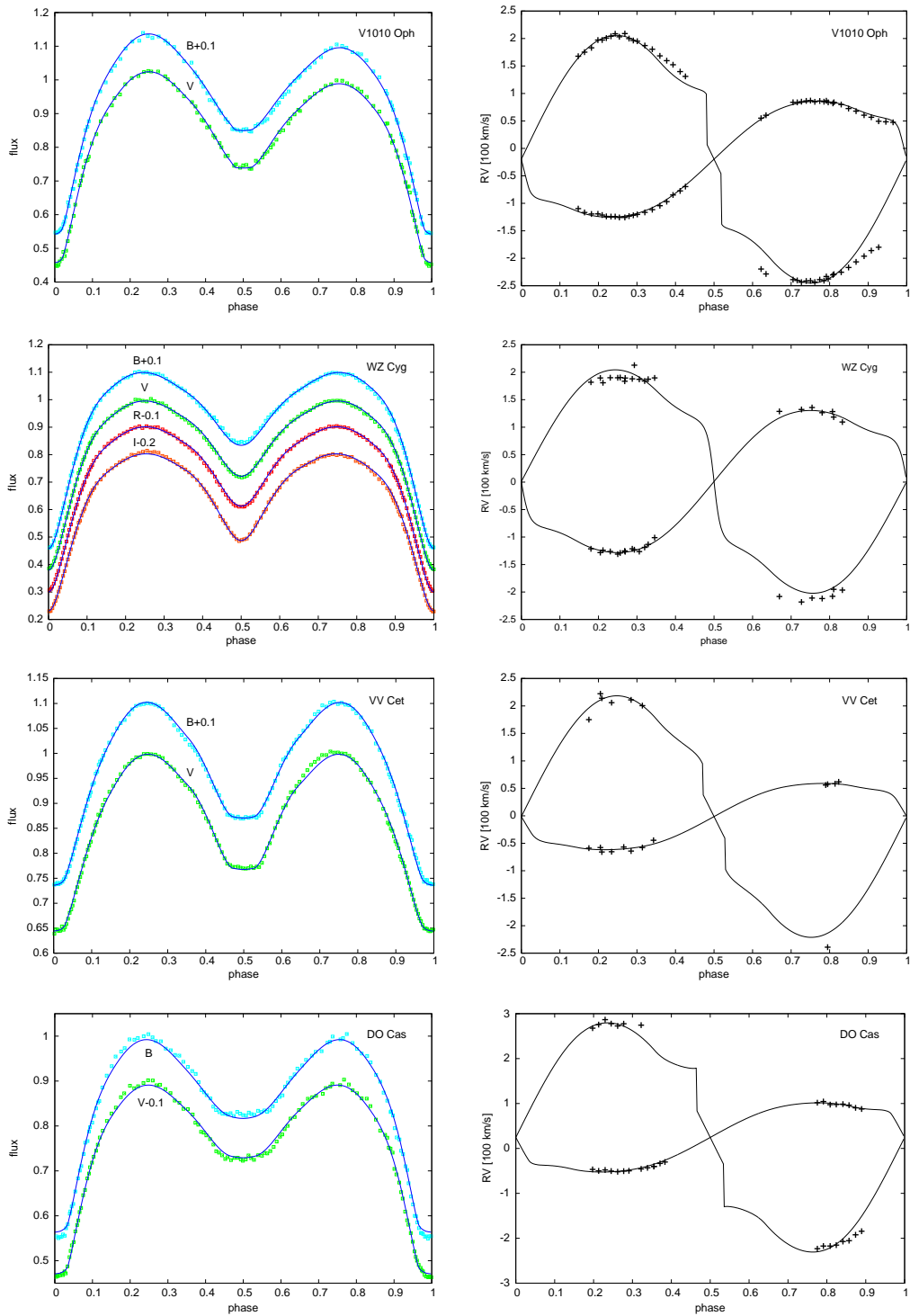


Fig. 1. Comparison between the observed and theoretical photometric (left panels) and RV (right panels) curves of V1010 Oph, WZ Cyg, VV Cet and DO Cas.

Table 5

General information concerning spectral classification of our targets.

system	method	spectral type	author(s)
WZ Cyg	spectral class.	F4V	Ogłóza & Rucinski (priv. comm.)
DO Cas	spectral class.	A4V	Ogłóza & Rucinski (priv. comm.)
BV Eri	spectral class.	F2V	Ogłóza & Rucinski (priv. comm.)
CN And	spectral class.	F5V	Rucinski et al. (2000)
BX And	spectral class.	F2V	Bell et al. (1990)
CX Vir	spectral class.	F5V	Hilditch & King (1988)
FT Lup	spectral class.	F2V	Hilditch et al. (1984)
FO Hya	B-V	F0V	Candy & Candy (1997), this work
FS Lup	B-V	G2V	this work
V747 Cen	B-V	A5V	Chambliss (1970)
VV Cet	B-V	A5V	Rahman (2000), this work
V1010 Oph	UV continuum	A7V	Corcoran et al. (1991)

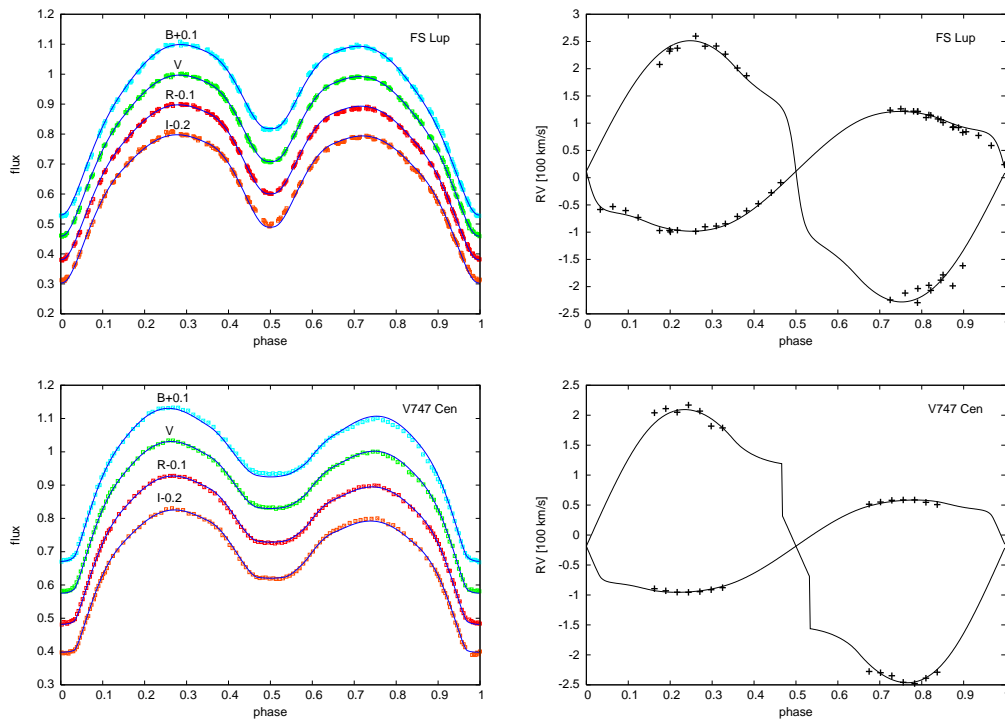


Fig. 2. Comparison between the observed and synthetic photometric (left panels) and RV (right panels) curves of FS Lup and V747 Cen.

Table 6

The results obtained from light- and RV-curve modelling of *near-contact* systems.

\* - parameters fixed during light curve modelling (see Sections 3 and 4 for explanations).

parameter	V1010 Oph	WZ Cyg	VV Cet	DO Cas	FS Lup	V747 Cen
$i[^{\circ}]$	86.14(37)	83.497(32)	81.89(13)	89.94(30)	82.64(23)	87.16(18)
$T_{\text{eff}}^{\text{prim}} [K]$	7500*	6530*	8150*	8350*	5860*	8150*
$T_{\text{eff}}^{\text{sec}} [K]$	5132(11)	4932(2)	6252(7)	4297(26)	5130(5)	4275(16)
$\Omega_{\text{prim}}$	2.81773*	3.1200(1)	2.43060*	2.4879(15)	2.8181(5)	2.51001*
$\Omega_{\text{sec}}$	2.8352(33)	3.1200(1)	2.4802(12)	2.4751(1)	2.8443(39)	2.5342(14)
$q_{\text{spec}}$	0.470(3)*	0.631(36)*	0.284(8)*	0.304(5)*	0.470(7)*	0.320(5)
$v_{\gamma} [km/s]$	-19.65(4)	1.05(88)	-1.36(90)	26.22(30)	11.64(63)	-18.55(46)
$a [R_{\odot}]$	4.487(15)	4.039(27)	3.006(41)	4.587(32)	2.746(16)	3.522(21)
$L_{1B}$	11.323(12)	10.4347(46)	11.5776(67)	12.3042(92)	10.227(15)	12.5055(64)
$L_{1V}$	10.960(14)	10.1042(44)	11.2295(70)	12.1172(99)	9.978(16)	12.2276(60)
$L_{1R}$	—	9.9063(42)	—	—	9.805(16)	11.9661(64)
$L_{1I}$	—	9.4824(41)	—	—	9.586(16)	11.7091(67)
$L_{2B}$	0.849(11)	1.5717(38)	1.0013(59)	0.1278(64)	2.404(16)	0.1346(43)
$L_{2V}$	1.122(13)	1.8488(39)	1.2078(63)	0.2092(88)	2.589(15)	0.2156(58)
$L_{2R}$	—	2.1257(40)	—	—	2.717(15)	0.3034(72)
$L_{2I}$	—	2.5910(38)	—	—	2.918(15)	0.4866(91)
$\phi[^{\circ}]$	90.0*	—	105.20(87)	—	93.7(2.0)	90.0*
$\lambda[^{\circ}]$	79.5(1.5)	—	0.4(1.5)	—	1.80(12)	41.0(1.2)
$r[^{\circ}]$	19.7(1.4)	—	14.744(97)	—	58.07(54)	64.7(2.0)
$T_{\text{spot}}/T_{\text{eff}}^{\text{sec}}$	1.378(31)	—	—	—	—	1.2094(40)
$T_{\text{spot}}/T_{\text{eff}}^{\text{prim}}$	—	—	0.253(79)	—	0.9136(10)	—

#### 4. Near-contact binary stars

##### 4.1. V1010 Oph

For light-curve modelling, we used the only available BV data obtained by Leung (1974). As an O’Connell effect is visible in the light curves, we also introduced a spot into the model. During computations, we observed good convergence of  $\Omega_1$  to a critical value of the first Lagrangian point  $L_1$ , and finally a semi-detached configuration was obtained as the best solution. This result naturally explains both the presence of the hot spot on the secondary star that is present in our model and the period shortening seen in the O–C diagram (Kreiner et al., 2001), as the result of mass transfer from the more massive primary to the less massive secondary. Although BFs (Fig. 3) were calculated from high signal-to-noise spectra, they did not reveal any features that could be interpreted as a hot spot. This may be a consequence of exceptional characteristics of this hypothetical spot in RV space, preventing it from being easily detected; or of insufficient spectral resolution; or of both these factors.

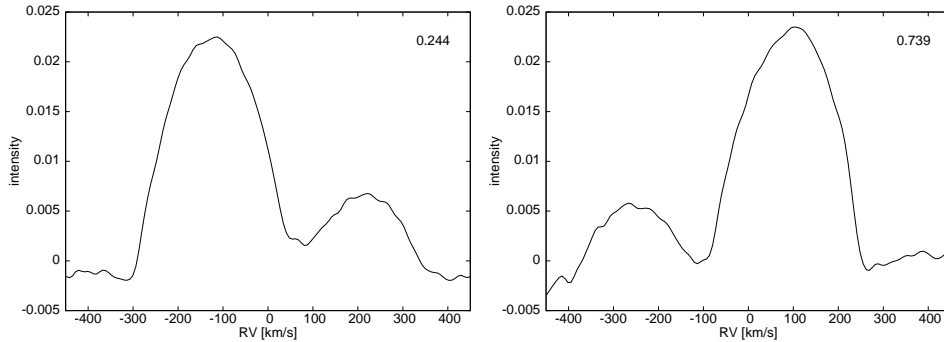


Fig. 3. BF profiles of V1010 Oph obtained with F2V RV standard in both quadratures. The phases calculated for the times of mid-exposure are given in the upper-right corner.

#### 4.2. WZ Cyg

We took a new set of light and RV curves over a two-month period. Despite many attempts, we were not able either to remove or to explain the significant differences among the values of  $v_\gamma$  determined separately for the RV curves of each component. High-resolution, good-SN spectra might resolve the ambiguity. Upon assuming a spectroscopic mass ratio of  $q_{\text{spec}} = 0.631(36)$ , we obtained a near-contact configuration (Table 6, Fig. 1) for this system. Because of the rather large uncertainty in  $q_{\text{spec}}$ , we made two additional light-curve models with two extreme possible values of  $q_{\text{spec}}$  (0.595 and 0.667), assumed constant in the computations. These models, however, likewise yielded a near-contact configuration.

#### 4.3. VV Cet

As the data obtained with the R filter turned out to be affected by instrumental problems, we used only the BV data during light curve modelling. As a result, we obtained a semi-detached configuration, with the primary component filling its Roche lobe. Only by placing a cold spot on the surface of the primary component was it possible to obtain a good fit to the observed light curves. Since the primary component has a radiative atmosphere, this result indicates the possibility that the primary is of type Ap. Unfortunately, our BF profiles are not of a quality high enough for us to detect and confirm the existence of such a spot on the star.

#### 4.4. DO Cas

As our three attempts to obtain new high-quality light curves failed, we used already-published BV data (Gleim & Winkler, 1969). Our light curve modelling used the spectroscopic mass ratio determined for the first time ( $q_{\text{spec}} = 0.304$ ) and resulted in a near-contact configuration.

#### 4.5. *FS Lup*

We decided to improve the spectral classification of FS Lup using our new data: a comparison of the spectra obtained at SAAO in the 3920–4750 Å region with respective spectra of RV standards indicated that the spectral type of FS Lup should be an early G. Additionally, from the  $B - V$  colour index, determined from our new photometric observations at the secondary minimum, we estimated the spectral type of the primary component as G2V (Table 5). The uncertainty deriving from the interstellar-reddening correction should not affect the effective temperature of the primary component (5860 K) by more than 150 K, as in the case of other systems with determined spectral types.

To account for the O’Connell effect, a cold spot on the primary component was placed in that model which best reproduced the observed light curves. BF profiles obtained from medium-resolution spectra seem to reveal a cold spot on the primary-star hemisphere facing the secondary star, at coordinates in accordance with those obtained from light-curve modelling. However, spectra of higher resolution are necessary to confirm this finding. In investigating configuration, we found FS Lup to be a near-contact system, possibly semi-detached, with the primary star almost or entirely filling its Roche lobe (Table 6).

#### 4.6. *V747 Cen*

The most interesting feature of V747 Cen is one which is, because of the high quality of our BFs, for the first time noticed in close binary systems: there is a well-defined region of increased intensity, visible in almost all profiles of the secondary component during second quadrature (Figs. 4, 5). We note that BFs of the secondary component in first quadrature are also higher in the vicinity of the primary component (as compared with the corresponding BF behaviour of V1010 Oph in Fig. 3). This brighter region is underlined only in the plot obtained at phase 0.190, but one can easily locate it on the remaining plots presented in the left column of Fig. 4. The region may be a result of a hypothetical stream of matter, leaving the primary star through the first Lagrangian point, undergoing a slight deflection through centrifugal force, and then directly striking the side of the secondary-star photosphere visible in first quadrature.

Light- and RV-curve modelling supported these conclusions: upon assuming that a hot spot on the secondary component is responsible for the O’Connell effect, we obtained a semi-detached configuration, with the primary component filling its Roche lobe (Table 6, Fig. 2).

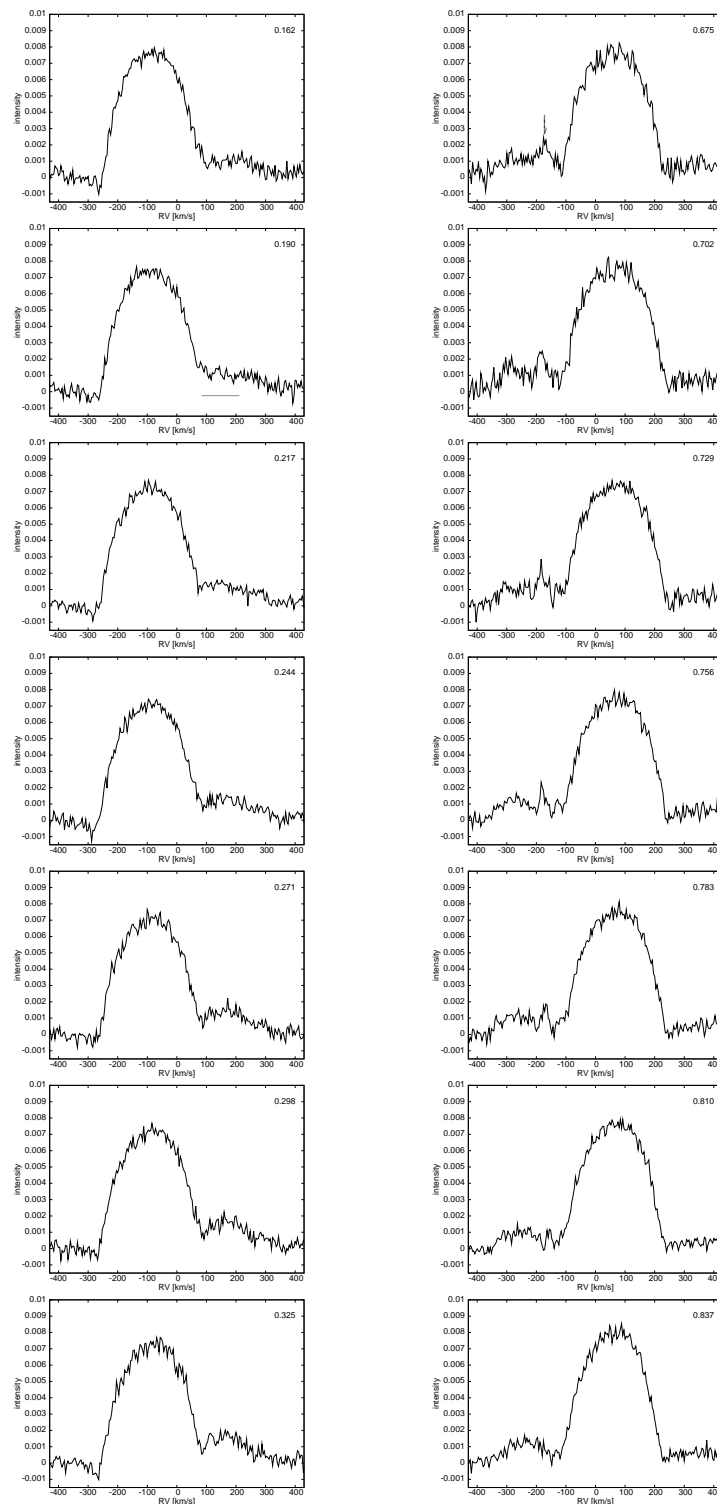


Fig. 4. BFs of V747 Cen obtained with G5V RV standard. The brighter region on the secondary component in the vicinity of the primary component is underlined at phase 0.190 (see Sec. 4.6). The well defined brighter region visible in second quadrature (right panels) is indicated by an arrow in the first plot. Only one BF profile of the secondary component, obtained at phase 0.837, seems to be free from accretion effects.

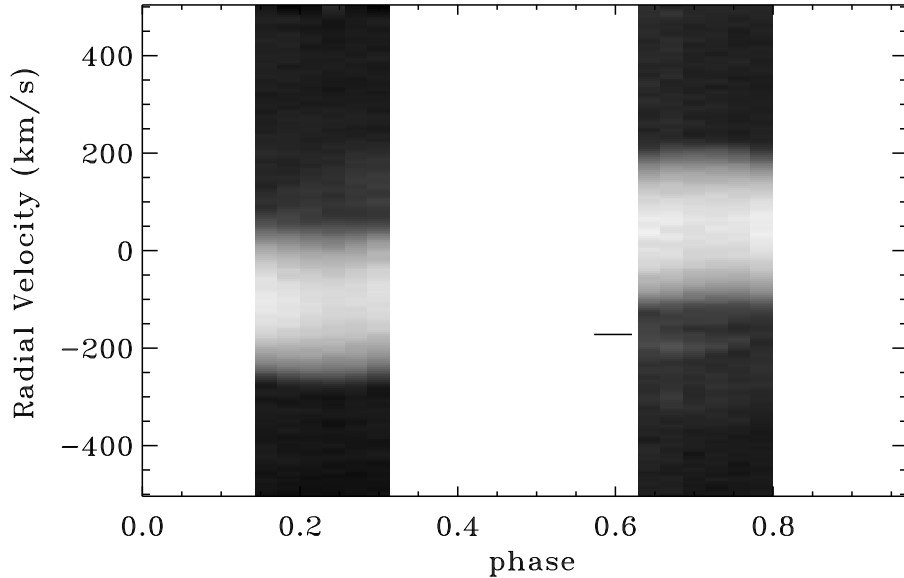


Fig. 5. BFs of V747 Cen (as in Fig. 4) in phase-velocity space, rebinned in phase with a constant increment of 0.03. The bright region on the secondary component visible in second quadrature is marked. As expected, the profile of the radiative A5V primary component does not reveal dark spots.

## 5. Contact systems with large $\Delta T$

### 5.1. *CX Vir*

In the high-quality BFs presented in Fig. 8, we notice even stronger differences between secondary-component velocity profiles obtained in first and second quadrature than for the semi-detached system V747 Cen (Sec. 4.6). At phases between 0.6 and 0.7, the triangular bright region (indicated by an arrow on the BF obtained at phase 0.747 in Fig. 8) dominates the signal of the secondary component. The latter begins to be distinguished from the brighter area in the BF obtained in phase 0.747 (Fig. 8, doubly underlined area on the same plot). The bright region becomes narrower and fainter with phase, but remains visible even at phase 0.844. BFs of the secondary component obtained in first quadrature are more intense (brighter) in the vicinity of the primary component (underlined area at phase 0.202), exactly as with V747 Cen. This similarly suggests an ongoing mass transfer from the primary to the secondary. In Fig. 9, a few cold spots (i.e., the darker coherent trails) on the primary are visible as well, outside the well defined bright region on the secondary star (indicated by longer marks).

As the bright region on the secondary component introduces the largest effects in the BFs, we assumed one circular hot spot on the equator of the secondary star during light-curve modelling. We expected to obtain a semi-detached configuration as in the case of V747 Cen, but in fact we obtained a contact configuration, with a

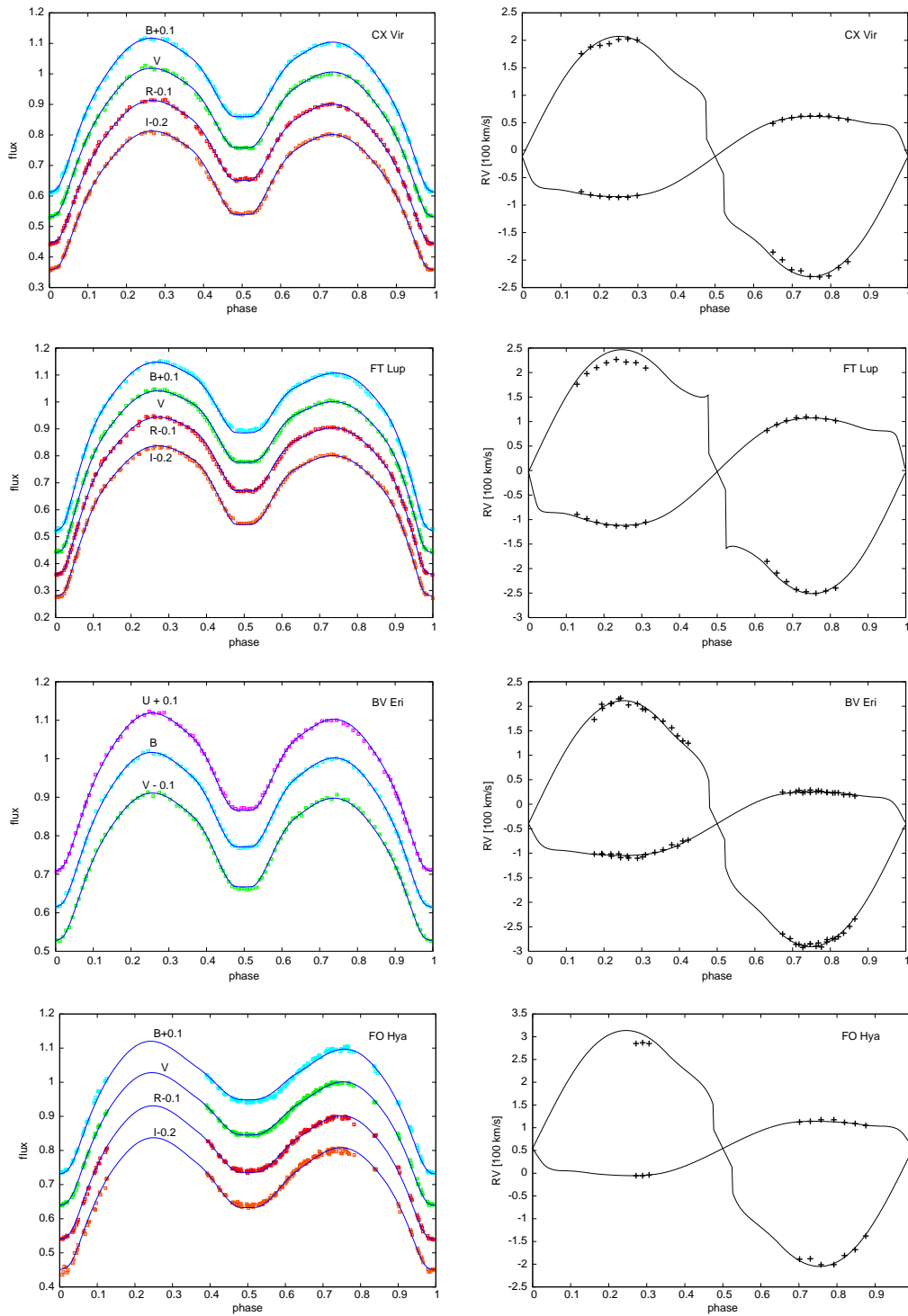


Fig. 6. Comparison between the observed and synthetic photometric (left panels) and RV (right panels) curves of CX Vir, FT Lup, BV Eri and FO Hya.



Table 7

The results obtained from light- and RV-curve modelling of contact systems with large temperature differences between components (CLdT).

\* - parameters assumed during light curve modelling (see Sections 3 and 5 for explanation)

parameter	CX Vir	FT Lup	BV Eri	FO Hya	CN And	BX And
$i[^{\circ}]$	83.33(17)	89.26(51)	80.31(11)	79.00(34)	69.416(92)	75.862(33)
$T_{eff}^{prim} [K]$	6450*	6700*	6700*	7000*	6450*	6650*
$T_{eff}^{sec} [K]$	4694(26)	4651(4)	5387(20)	4667(27)	4726(34)	4758(5)
$\Omega$	2.5146(8)	2.7231(3)	2.3737(7)	2.2714(25)	2.6403(12)	2.7760(5)
$q_{spec}$	0.343(3)*	0.440(3)*	0.274(2)*	0.238(6)*	0.385(5)*	0.455(8)*
$v_{\gamma} [km/s]$	-11.65(32)	-2.30(30)	-39.62(35)	54.42(30)	-23.47(63)	-24.00(60)
$a [R_{\odot}]$	4.584(19)	3.537(13)	3.365(12)	3.184(21)	3.163(22)	4.424(36)
$f [\%]$	21.2	13.4	20.0	36.0	3.0	4.5
$L_{1U}$	—	—	8.798(40)	—	—	—
$L_{1B}$	9.350(51)	10.597(23)	8.920(40)	10.746(81)	9.952(18)	11.0925(51)
$L_{1V}$	9.242(48)	10.315(24)	8.748(37)	10.886(78)	9.830(16)	10.8293(52)
$L_{1R}$	9.039(49)	10.164(24)	—	11.091(74)	9.710(15)	10.6043(56)
$L_{1I}$	8.956(47)	9.909(22)	—	11.093(96)	9.531(13)	10.2546(58)
$L_{2U}$	—	—	0.996(23)	—	—	—
$L_{2B}$	0.648(26)	0.7151(46)	0.946(22)	0.361(13)	0.781(36)	0.9154(52)
$L_{2V}$	0.789(30)	0.9002(56)	1.093(23)	0.497(16)	0.946(40)	1.1300(58)
$L_{2R}$	0.923(32)	1.0850(61)	—	0.630(18)	1.114(43)	1.3325(61)
$L_{2I}$	1.185(35)	1.3902(69)	—	0.759(19)	1.395(44)	1.6874(60)
$l_{3U}$	—	—	0.1407(30)	—	—	—
$l_{3B}$	0.1060(35)	0.0481(16)	0.1409(30)	0.0894(63)	—	—
$l_{3V}$	0.1048(34)	0.0463(18)	0.1398(29)	0.0672(60)	—	—
$l_{3R}$	0.1073(37)	0.0456(18)	—	0.0374(58)	—	—
$l_{3I}$	0.0957(37)	0.0386(16)	—	0.0304(74)	—	—
$\phi[^{\circ}]$	90.0*	90.0*	90.0*	90.0*	90.0*	90.0*
$\lambda[^{\circ}]$	7.61(29)	19.66(43)	11.83(35)	64.9(3.8)	11.49(36)	3.00(0.45)
$r[^{\circ}]$	104.1(2.1)	65.3(1.3)	107.9(1.8)	102.9(4.4)	113.9(1.9)	19.53(0.91)
$T_{spot}/T_{eff}^{sec}$	1.2051(59)	1.2053(33)	1.141(4)	1.1015(55)	1.2138(72)	1.177(15)

large temperature difference between components and a significant value of third light  $l_3$ , comprising about 10% of the total flux (Table 7). Hilditch & King (1988) did not account for a third light in their analysis, as it is not obvious from their data whether the secondary minimum is total or partial. This apparently small detail always, however, has a large impact on the final light-curve solution.

### 5.2. FT Lup

As in the case of V747 Cen and CX Vir, the BF profiles of the secondary component obtained in second quadrature reveal a bright region. In first quadrature, the BF profiles of the secondary are brighter in the vicinity of the primary (Fig. 10; for detailed explanations, check particularly the plots obtained at phases 0.233 and

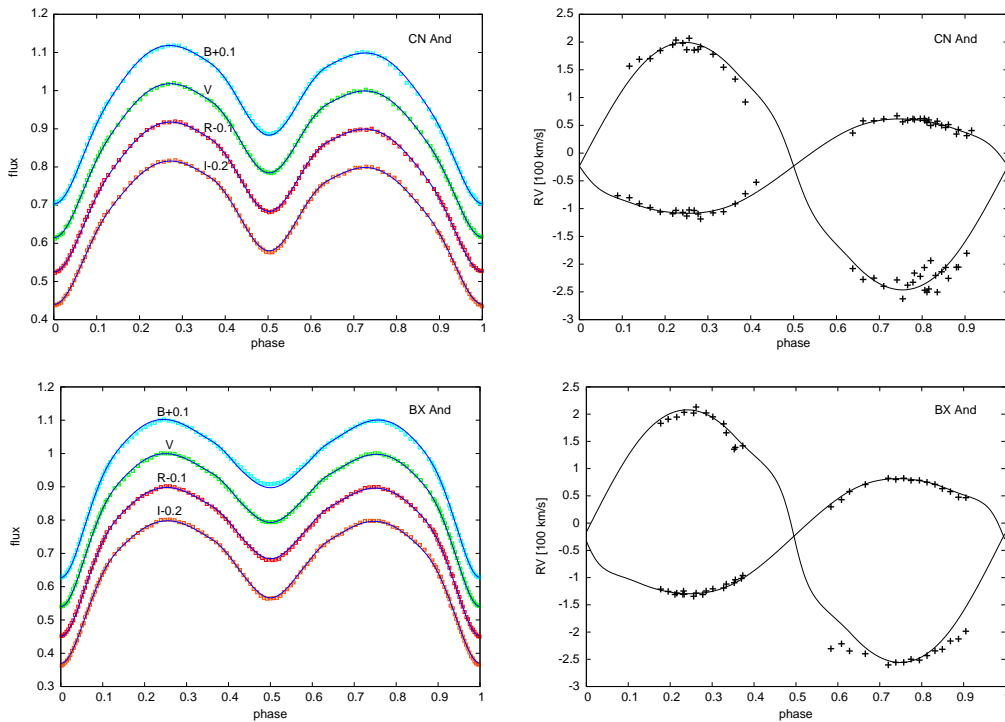


Fig. 7. Comparison between the observed and synthetic photometric and RV curves of CN And and BX And.

0.710). In Fig. 11, we display the BFs in the phase-RV plane. Here one can clearly see not only the track of the bright region (hot spot) in second quadrature but also several tracks of cold spots on the primary in both quadratures.

Accretion processes between components considerably disturb the RV curve of the secondary, with  $v_\gamma$  as obtained from the RV curve of the secondary 10 km/s smaller than the  $v_\gamma$  obtained from the apparently undisturbed RV curve of the primary. We consequently determined the spectroscopic mass ratio of this system using only the secondary-component RV measurements obtained at second quadrature (Fig. 6). At these phases (Fig. 10, right panels), the influence of the well defined bright region can be easily taken into account during the RV measurement process.

With a hot spot on the secondary component, we expected to obtain a semi-detached configuration from light curve modelling. However, as in the case of CX Vir, our best solution converged at the contact configuration with large  $\Delta T$  between components and a non-negligible (4%-to-5%) contribution from a third light (Table 7).

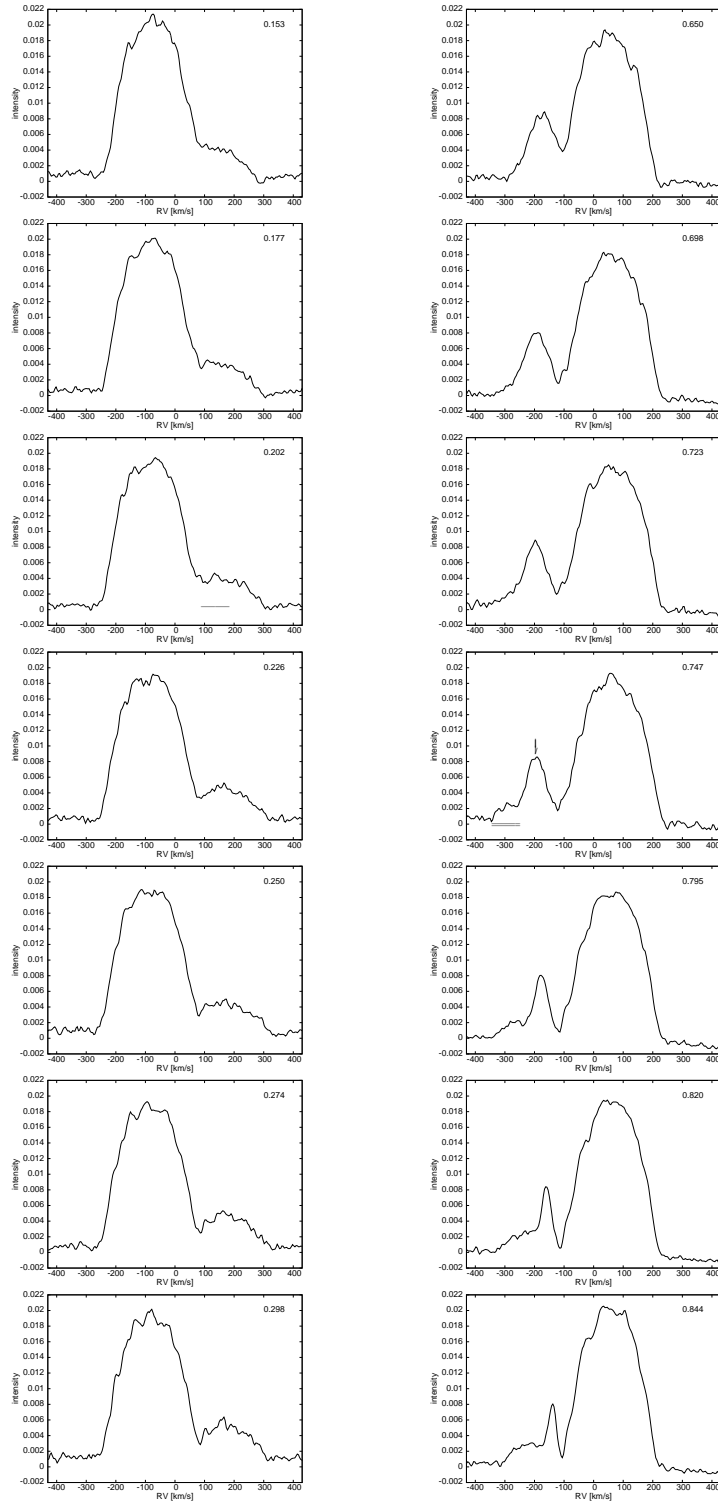


Fig. 8. BFs of CX Vir obtained with F5V RV standard. The brighter region on the secondary component in the vicinity of the primary component is underlined at phase 0.202 (see Section 5.1). The well defined very bright region visible at second quadrature (right panels) is indicated by an arrow on the BF obtained at phase 0.747, at which point it begins to be distinguishable from the apparently pure profile of the secondary component (doubly underlined on the same plot). The outstanding accuracy of the BF profiles is noteworthy here.

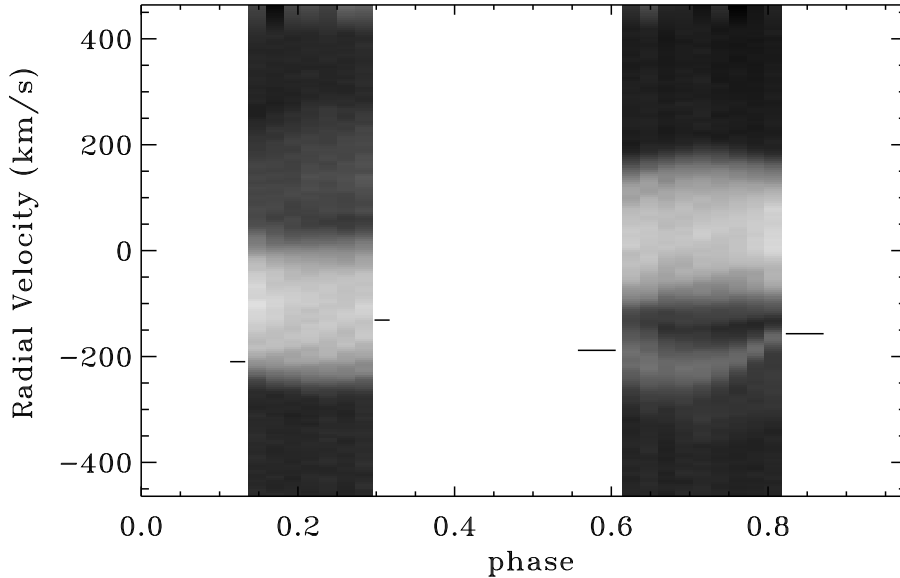


Fig. 9. BFs of CX Vir in phase-velocity representation, rebinned in phase with a constant increment of 0.0235. In addition to the very bright region on the secondary component seen in second quadrature (as indicated by longer marks), cold spots on the primary component are visible. (One of these, near first quadrature, is indicated by shorter marks).

### 5.3. *BV Eri*

The BF profiles of BV Eri again reveal a well defined brighter region on the secondary component (Fig. 12), although not as clearly as in three systems previously discussed. Similarly, in first quadrature the BF profiles of the secondary are also brighter in the vicinity of the primary-component profile.

To perform light-curve modelling, we used the only available very good-quality UBV data, published by Badee et al. (1983). In the model, we assumed a hot spot on surface of the secondary component responsible for the O’Connel effect and for the features discovered in the BFs. Our computations resulted in a contact configuration with large  $\Delta T$  and with a significant (13% to 14%) contribution from a third light.

### 5.4. *FO Hya*

Our new  $BV(RI)_c$  data confirmed the F0V spectral type of the primary component determined by Candy & Candy (1997). First RV curves yielded a considerably smaller value of the mass ratio ( $q_{\text{spec}} = 0.238$ , in contrast with the value  $q_{\text{phot}} = 0.552$  which Candy & Candy determined). Despite the relatively poor quality of the spectra obtained at LCO, we additionally notice differences between the BF profiles of the secondary component obtained in both quadratures: the profiles appear brighter and are well defined in first quadrature, being considerably weaker

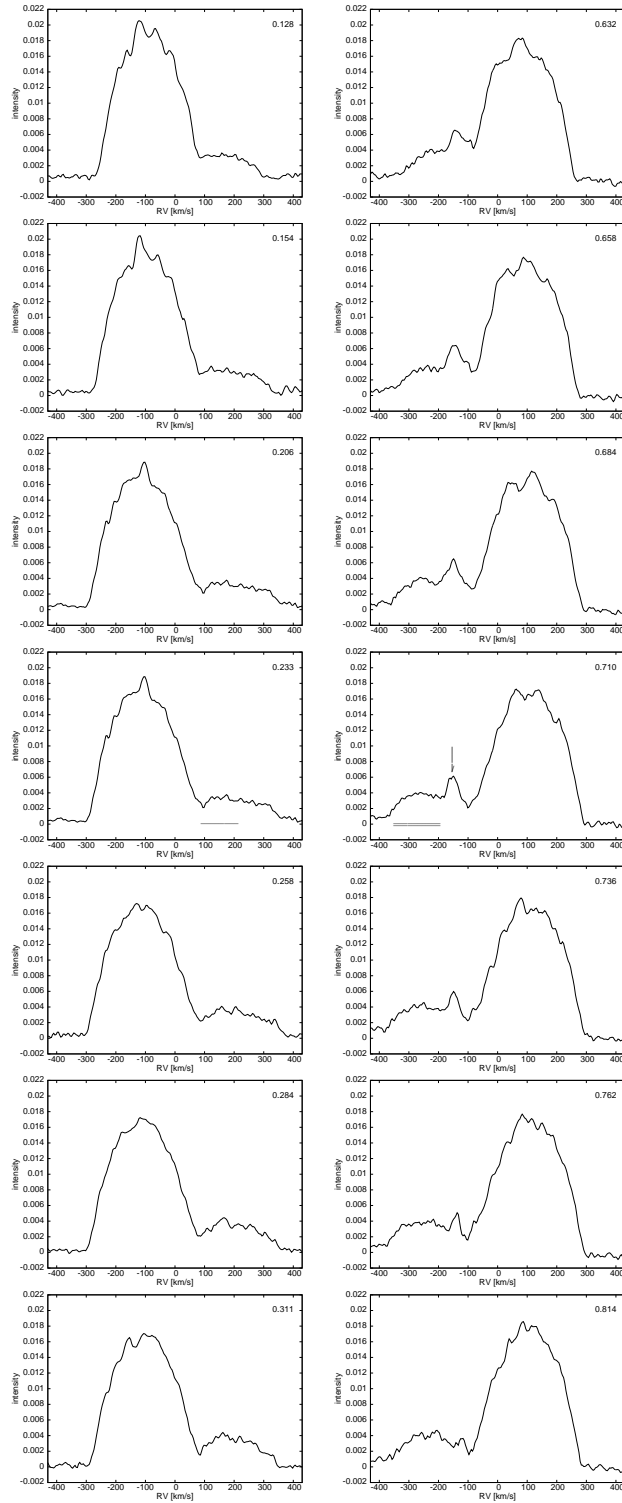


Fig. 10. BFs of FT Lup obtained by means of F2V RV standard. The region of increased intensity on the secondary component in the vicinity of the primary component is underlined in phase 0.233 (see Section 5.2). The well defined high-intensity region visible in second quadrature (right panels) is indicated by an arrow on the BF obtained at phase 0.710, with the apparently pure profile of the secondary component doubly underlined on the same plot.

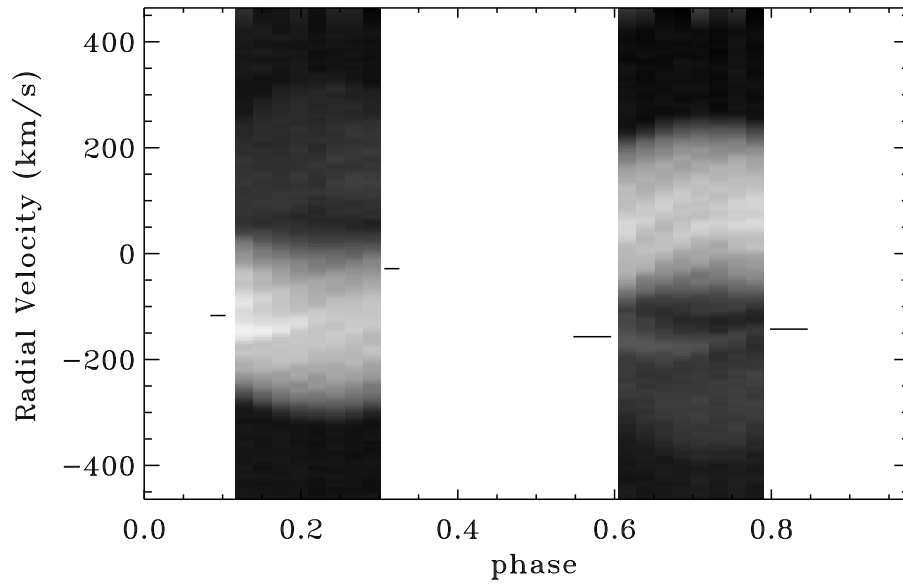


Fig. 11. BF<sub>s</sub> of FT Lup in phase-velocity representation, rebinned in phase with a constant increment of 0.025. In addition to the well defined region of increased intensity on the secondary component in second quadrature (indicated by longer marks), a few cold spots on the primary are visible. (One of these is indicated by shorter marks in first quadrature.)

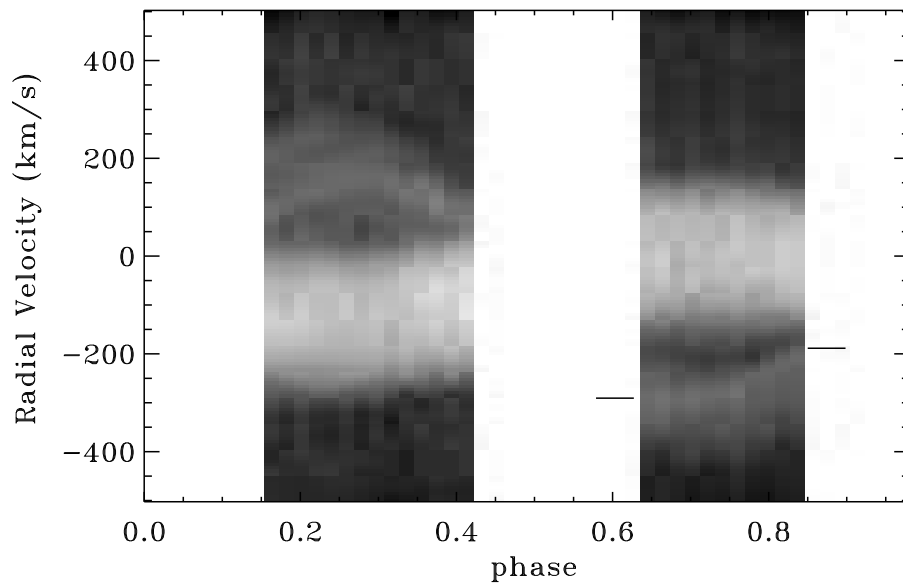


Fig. 12. BF<sub>s</sub> of BV Eri in phase-velocity representation, rebinned in phase with a constant increment of 0.02. The well defined bright region of increased intensity on the secondary component (indicated by marks) is visible at phases in second quadrature.

in second quadrature. The profiles obtained before phase 0.75 seem to reveal a region of increased intensity, as with the four systems discussed above.

Because the incompleteness of the new light curve deprived us of evidence for an O’Connell effect, we first attempted to model the light curves without spots. This first model, however, did not yield a good fit. In our second attempt, using information obtained from BF profiles and following Candy & Candy (1997), we introduced a hot spot on the secondary. The model from these computations, while yielding a reasonably good fit (Fig. 6), additionally delivered a contact configuration, a large  $\Delta T$  between the components, and a considerable contribution from a third light (Table 7).

### 5.5. *CN And*

CN And is a very frequently observed and analyzed system, and different configurations were obtained from its light and RV curve modelling (Table 1). As almost all available archival light curves of CN And are of low quality, we decided to obtain new high-precision, multicolour (BVRI) data. Radial velocity curves were already obtained at DDO, and the spectroscopic mass ratio was derived by the BF method (Rucinski et al. 2000). In Fig. 13 we display binned BFs of CN And in the phase-velocity plane. The BFs, although individually rather noisy, give information of better quality when stacked, revealing a subtle track of a brighter region on the secondary component at second quadrature. We therefore decided to explain the O’Connell effect apparent in light curves by assuming one large hot spot on the secondary component. We obtained a marginal-contact configuration with large  $\Delta T$ . However, in contrast with CX Vir, FT Lup, BV Eri, and FO Hya, it was not necessary to include a third light to obtain a good fit.

We note that Zola et al. (2005) obtained a semi-detached configuration. Their model, however, assumed two cold spots on the primary component, whereas in our model a hot spot was placed on the surface of the secondary, in agreement with information obtained from BFs.

### 5.6. *BX And*

At first glance, our new BVRI light curves appeared to be free from an O’Connell effect. However, synthetic light curves obtained within a spotless model (yielding a contact configuration with  $f = 10\%$  and large  $\Delta T$  between components) did not fit the observed curves very well, with the discrepancy becoming especially pronounced around the secondary minimum. A closer inspection of the region around phase 0.3 reveals that it is slightly brighter than the one around phase 0.7. The assumption of a hot spot on the equator of the secondary component yielded a marginal-contact configuration with  $f = 4.5\%$  and large  $\Delta T$  (Table 7), but with about 40% smaller  $\chi_{\text{red}}^2$ .

In order to validate the assumption of a hot spot in our model, we examined the available BF profiles obtained from medium-resolution spectra, but they did not

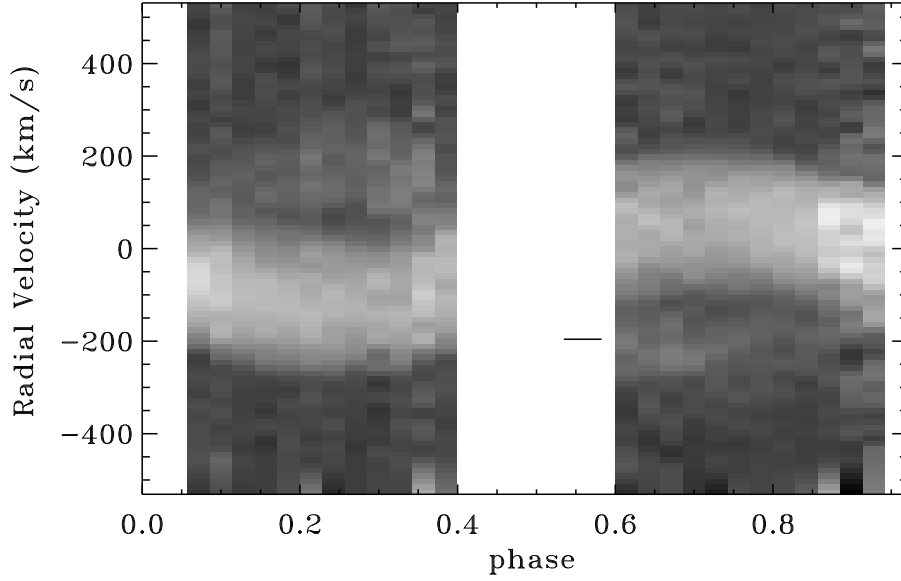


Fig. 13. BFs of CN And in phase-velocity representation, rebinned in phase with a constant increment of 0.03. The mark indicates the brighter region on the secondary component visible at second quadrature in the phase range 0.6-0.8.

show any visible tracks of a hot spot on the secondary component. This outcome may be due to the small size of the spot (as obtained from light curve modelling), with detection perhaps only possible through BFs derived from high-resolution spectra.

Table 8

Physical parameters of components derived from light- and RV-curve modelling.

system	$M_1[M_\odot]$	$M_2[M_\odot]$	$R_1[R_\odot]$	$R_2[R_\odot]$	$T_1[K]$	$T_2[K]$	$L_1[L_\odot]$	$L_2[L_\odot]$
V1010 Oph	1.887(19)	0.887(15)	2.01(3)	1.40	7500	5132	11.45	1.22
WZ Cyg	1.589(32)	1.003(37)	1.70(4)	1.37	6530	4932	4.71	1.00
VV Cet	1.042(43)	0.296(20)	1.48(5)	0.79	8150	6252	8.66	0.85
DO Cas	2.130(45)	0.650(25)	2.22(4)	1.29	8350	4297	21.47	0.51
FS Lup	1.301(23)	0.611(20)	1.23(3)	0.85	5860	5130	1.60	0.45
V747 Cen	1.541(28)	0.493(17)	1.70(3)	0.98	8150	4275	11.42	0.29
CX Vir	1.731(21)	0.594(13)	2.24(3)	1.39	6450	4694	7.78	0.84
FT Lup	1.871(21)	0.823(15)	1.64(2)	1.13	6700	4651	4.86	0.54
BV Eri	1.560(17)	0.430(07)	1.70(2)	0.96	6700	5387	5.22	0.70
FO Hya	1.588(61)	0.378(34)	1.67(3)	0.89	7000	4667	5.68	0.33
CN And	1.433(30)	0.552(20)	1.48(3)	0.95	6450	4726	3.40	0.40
BX And	2.148(52)	0.977(41)	2.01(5)	1.40	6650	4758	7.08	0.90



## 6. Physical parameters of components

Using the results obtained from light- and RV-curve modelling (Table 6 and Table 7), we computed physical parameters of components (Table 8). Because the highly distorted components of contact binary stars significantly differ from a sphere, their effective radii  $R$  were calculated under the assumption that the surface area of each component is equal to the surface area of a spherical star of radius  $R$ . As the radii are scaled by their respective distances  $a$  between centres of masses of components,  $a$ -errors propagate accordingly on the radii of both components. Effective temperatures of primary components derived from spectral classification are known with an accuracy no better than 100–200 K, and these external errors, much larger than those obtained from light-curve modelling alone (Table 6 and Table 7), affect also the effective temperatures of secondary components. These uncertainties make it even more difficult to estimate errors in the luminosity  $L$ , but  $L$  errors are usually equal to 10% to 30% of  $L$  values (Yakut & Eggleton, 2005).

Zola et al. (2006) considered a sample of contact binary systems for which physical parameters were derived from combined light- and RV-curve modelling. From the available data, they constructed mass–radius (M–R), mass–luminosity (M–L) and temperature–luminosity (T–L) diagrams. The M–L and T–L diagrams were also constructed using component physical parameters corrected for the effect caused by energy transfer from the primary to the secondary, by applying equations from Mochnacki (1981), with an ad-hoc modification taking into account temperature differences between components (Zola et al., 2006). Theoretical parameters of stars on ZAMS, TAMS, and hydrogen depletion in the core were computed with the EZ program (Paxton, 2005), which is based on the most recent version of Eggleton’s STARS code (Pols et al., 1995).

We have appended to the above-mentioned diagrams the physical parameters of the systems analyzed in this work (Table 8). As can be seen in the M–R diagram (Fig. 14), almost all primary components of our targets (the only exception is VV Cet) have parameters corresponding to the MS stars, while secondary components are oversized by a factor similar to those of components of W UMa-type systems.

In Figure 15, we present two T–L diagrams. The first is constructed with the physical parameters from Table 8, while the second uses parameters corrected for an effect caused by an energy transfer between components. While the uncorrected parameters of the CLdTs secondary components (red squares) do not differ from those of the secondary components of near-contact systems taken from literature, in the second plot they show an obvious tendency to occupy the region avoided by secondary components of W UMa type systems. This matter will be discussed more thoroughly in the next section.

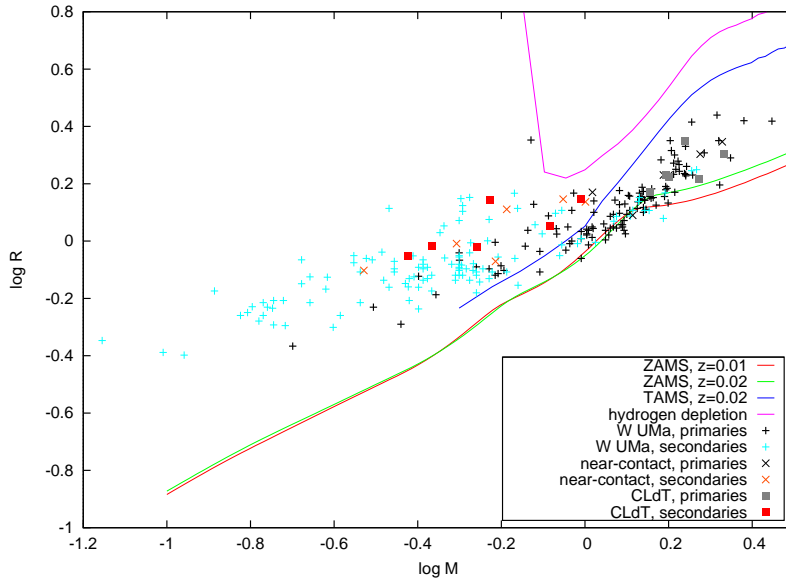


Fig. 14. The M–R diagram for systems analyzed in this work on the background of the sample of W UMa-type stars from Zola et al. (2006). The continuous line represents the theoretical lines of ZAMS and TAMS computed for metallicities of  $z = 0.01$  and  $z = 0.02$ . “Near-contact” denotes the systems described in Sections 4.1–4.6, and “CLdT” the systems described in Sections 5.1–5.6. Physical parameters of these systems are listed in Table 8.

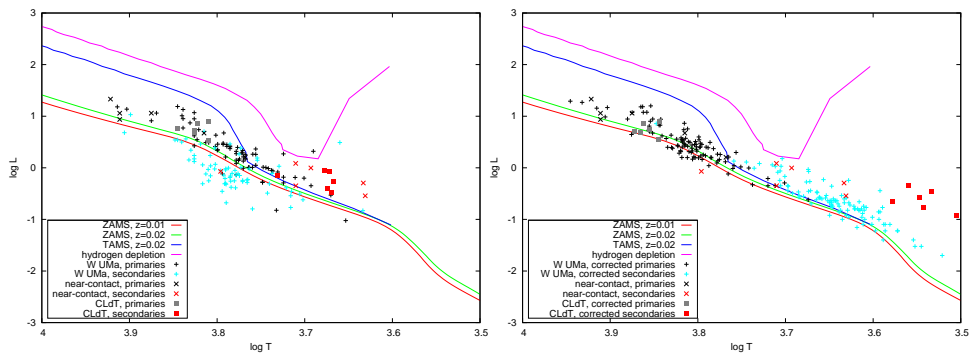


Fig. 15. T–L diagrams for systems analyzed in this work, without (left panel) and with (right panel) provision for effects of energy transfer. Parameters of the W UMa-type stars in the sample from Zola et al. (2006) are also shown. The second plot indicates that secondary components of CLdT systems lie in the region which secondary components of W UMa-type systems tend to avoid.

## 7. Discussion and conclusions

We performed light- and RV-curve modelling of twelve close binary stars, for which contact configurations with large temperature differences between components have been reported at least once in the literature. In our analysis we applied new spectroscopic mass ratios, obtained through the BF method, determined for the first time for all systems but CN And.

We obtained a near-contact configuration for V1010 Oph, WZ Cyg, VV Cet, DO Cas, FS Lup, and V747 Cen. The primary components of V1010 Oph, WZ Cyg, VV Cet, FS Lup, and V747 Cen fill (or nearly fill) their Roche lobes, and accordingly their secondaries are considerably oversized; an ongoing or past mass transfer can explain their larger radii according to the mechanism proposed by Webbink (1976) and Sarna & Fedorova (1989). In this configuration, an ongoing mass transfer should cause period shortening, but this is only confirmed in the O–C diagram of V1010 Oph (Kreiner et al., 2001).

Among systems from this group, the most interesting results were obtained for V747 Cen and FS Lup. The latter appears to be the second-known short-period period (0.38 d) semi-detached system, which next to V361 Lyr (Hilditch et al., 1997), is captured in a broken-contact stage of oscillation, as predicted by the TRO theory (see Section 1), or during the phase of a first-time approach to a contact phase. In the high-quality BFs (i.e., stellar images in velocity space) of V747 Cen, we discovered bright regions on the secondary component. The discovery is a sign of one or more hot spots, most probably a result of accretion occurring between the stars. This picture is in full accordance with the result obtained from light- and RV-curve modelling, which resulted in a semi-detached configuration for this system.

From the light- and RV-curve modelling of CX Vir, FT Lup, BV Eri, FO Hya, CN And, and BX And, we obtained contact models with large temperature differences between components ( $\Delta T > 1000$  K), in contradiction to theoretical predictions for contact systems. However, as in the case of V747 Cen, the most interesting results for CX Vir, FT Lup, BV Eri, FO Hya, and CN And were obtained from discovery of hot spots in BFs of their secondary components. As the existence of the hot spots can be explained only by accretion effects occurring between components, that discovery strongly supports semi-detached rather than contact configurations for these systems.

The just-stated direct result aside, there additionally are indirect indications of the possibility that (at least some) contact models with large  $\Delta T$ , obtained from light- and RV-curve modelling, are wrong.

(1) From light-curve modelling of four systems with the strongest bright regions, we also obtained significant values of third light (Sections 5.1–5.4, and Table 7). The hypothetical third component is neither visible in BFs (as a slowly rotating sharp-line star) nor as a nearby field star in DSS images of these systems. However, without adding a third light into the model as adjusted parameter, in all

cases flat secondary minima and depth of primary minima were not reproduced well by these models, and as a consequence the obtained  $\chi_{\text{red,weigh}}^2$  were at least a few dozens of percent higher. It is also worth noting that the bright regions are common features not only for CX Vir, FT Lup, BV Eri, FO Hya and CN And, but also for V747 Cen, for which light- and RV-curve modelling gave a semi-detached configuration without any third light, in full consistency with all the information inferred from its BFs. On this empirical basis, one may deduce that all the systems are in fact semi-detached, with the duality of configurations obtained within a pure Roche-lobe model resulting from accretion processes taking place on different levels in the various individual systems.

(2) The BFs of secondary components obviously appear different in the two quadratures. Whereas in first quadrature they do possess a characteristic smoothly increasing intensity toward primary components (this can be explained as a result of star-stream interaction producing a hot spot and causing considerable velocity turbulence), the well defined bright regions in second quadratures can be produced by returning streams encircling secondary components. If this is a correct picture, then these systems must be semi-detached. The positive (in absolute sense) departures of RVs of secondary components from the Roche model, observed in the case of V1010 Oph, DO Cas (Fig. 1, right panel) and BX And (Fig. 7, right panel), in phases close to both minima, may be a sign of such high-velocity streams. Unfortunately, other systems were observed only during phases close to quadratures.

(3) According to the O–C diagrams (Kreiner et al., 2001), continuous period shortening of FT Lup and CN And argues for a semi-detached configuration allowing for mass transfer from primary to secondary components. This empirical fact is consistent with information extracted from BFs of these systems, but it is inconsistent with configurations obtained from light-curve modelling. CX Vir, BV Eri, FO Hya, and BX And do not reveal any obvious signs of a permanent period decrease or increase. The latter is expected to be easily observable in O–C diagrams of contact systems with large temperature differences, as the mass transfer rate from secondary to primary star in common envelope is predicted to be of order  $10^{-8}M_{\odot}/\text{yr}$  (Flannery (1976), Robertson & Eggleton (1977)). The lack of permanent period increase in this group of systems is again in contradiction to the supposition of contact configurations.

(4) The position on the T–L diagram of secondary components of contact systems with large  $\Delta T$ , constructed from their physical parameters as corrected for effects of energy transfer in a common envelope (Fig. 15, right panel) indicates that these stars differ significantly from the components of typical W UMa-type systems. If their input physical parameters (Table 8) obtained within a false contact model from the WD code are wrong (due to the problems with unexplained sources of  $l_3$ ), the corrections for energy transfer may in turn lead to very different output values, as observed in Figure 15 (right panel).

(5) The discovery of bright regions in BFs of secondary components, the ob-

servation of significant differences in BF profiles in the two quadratures, and the discovery of spotted primaries in (at least) CX Vir and FT Lup (as described in Sections 5.1–5.5) suggests that it may not be possible to derive accurate configurations from light-curve modelling. This is because smoothly varying EW- and EB-type light curves contain only information about changes of integrated binary-star light with phase, offering constraints too weak to yield a model consistent with the whole range of information extracted from spectroscopy. The modelling software based on the Roche model cannot properly handle all these effects, because there remains a large set of free parameters: our attempts to obtain much more reliable models of CX Vir, FT Lup, and CN And did not deliver unique fits.

Although all the above findings strongly support the hypothesis of Rucinski (1986) and Eggleton (1996), that systems for which Roche-lobe-based computer models give contact configurations with  $\Delta T > 1000$  K are in fact semi-detached (see Section 1), further observations are necessary for full confirmation of this finding. Doppler-imaging observations, as made by Pribulla & Rucinski (2008) for AW UMa, may be needed. The cited observations have revealed that the secondary component has the aspect of a small core-like star surrounded by optically thick matter. Further, the recent discovery of a double-peaked  $H_\alpha$  line in a short-period (1.6 d) SV Cen (Siwak et al., 2009) and (0.42 d) TYC 2675-663-1 W UMa type systems (Caballero-Garcia et al., 2010) may indicate an existence of accretion disk around one component, and a semi-detached rather than a contact configuration. This is a possibility previously envisaged by Zola (1995). The echelle spectra of CX Vir and FT Lup, covering a wide spectral range (UV–IR), do not reveal emission components in hydrogen lines. Further progress on contact-binary systems with large  $\Delta T$  between components may consequently be obtained from modelling of the available and the prospective new BFs, obtained over a whole orbital period.

**Acknowledgements.** The service-mode observations made at the ESO La Silla have been financed by the Optical Infrared Coordination Network (OPTICON), a major international collaboration supported by the Research Infrastructures Programme of the European Commission’s Sixth Framework Programme.

The observations at the David Dunlap Observatory and at the South African Astronomical Observatory have been financed by research funds of the Astronomical Observatory of the Jagiellonian University, the Polish Foundation for Astronomy, and the Polish Foundation of SALT. The observations at Las Campanas have been financed by a Canadian Space Agency grant to Prof. Slavek M. Rucinski within the CSA Space Science Enhancement Program.

MS and DKW appreciate the help and the hospitality of SAAO staff during observations, especially on the part of Mr. Fred Marang, Mr. Francois van Wyk, and Ms. Melony Spark.

MS especially acknowledges the following:

- Prof. Slavek M. Rucinski, for access to DDO observing facilities, for many discussions concerning the BF method and modern results in contact-binaries work, and for stimulating discussion of this paper;
- Prof. Jerzy Kreiner and the Mount Suhora Astronomical Observatory staff, for frequent access to observing facilities;
- Dr. Maria Kurpińska-Winiarska, Dr. Maciej Winiarski, Dr. Waclaw Waniak, and Dr. Andrzej Baran, for comments and advice concerning details of stellar photometry and spectroscopy;
- the ESO-La Silla technical staff and astronomers, for executing observing blocks during service-mode observations, and especially for taking excellent data;
- Ms. Heide de Bond, Mr. Jim Thompson, and Dr. Toomas Karmo, for their night assistance during observations at DDO;
- the Las Campanas Observatory technical staff, for day work, and Herman Olivares and Javier Huentes, for night assistance;
- the Canadian Space Agency, for a post-doctoral grant to Prof. Slavek M. Rucinski within the CSA Space Science Enhancement Program;
- Dr. Toomas Karmo and Mr. Bryce Croll for language corrections.

This paper reports the most important results obtained during the preparation of the MS PhD thesis, with SZ as thesis advisor.

## REFERENCES

- Badee, D., Duerbeck, H.W., Karimie, M.T., Yamasaki, A. 1983, *Ap&SS*, **93**, 69.
- Balona, L.A. 2000, *XLUZY: Photometer control and data acquisition*, SAAO.
- Baran A., Zola S., Rucinski S.M., Kreiner J.M., Siwak M., Drozd M. 2004, *AcA*, **54**, 195.
- Barone, F., Covino, E., Di Fiore, L., Milano, L., Russo, G. 1991, *Ap&SS*, **183**, 117.
- Barone, F., Di Fiore, L., Milano, L., Pirozzi, L., Russo, G. 1992, *Ap&SS*, **198**, 321.
- Bell, S.A., Rainiger, P.P., Hill, G., Hilditch, R.W. 1990, *MNRAS*, **244**, 328.
- Caballero-García, M.D., Torres, G., Ribas, I., Rísquez, D., Montesinos, B., Mas-Hesse, J.M., Domingo, A. 2010, *A&A*, **514**, 36.
- Candy, M.P., Candy, B.N. 1997, *MNRAS*, **286**, 229.
- Chambliss, C.R. 1970, *AJ*, **75**, 731.
- Claret, A., Diaz-Cordoves, J., Gimenez, A. 1995, *A&AS*, **114**, 247.
- Corcoran, M.F., Siah, M.J., Guinan, E.F. 1991, *AJ*, **101**, 1828.
- Diaz-Cordoves J., Claret A., Gimenez A. 1995, *A&AS*, **110**, 329.
- Eggen, O.J. 1967, *MmRAS*, **70**, 111.
- Eggleton, P.P. 1996, *ASPC*, **90**, 257.
- Flannery, B.P. 1976, *ApJ*, **205**, 217.
- Gleim, J.K., Winkler, L. 1969, *AJ*, **74**, 1191.
- Gu, S. 1999, *A&A*, **346**, 437.
- Gray, R.O. 2001, <http://phys.appstate.edu/spectrum/spectrum.html>, Department of Physics and Astronomy, Appalachian State University.
- Harmanec, P. 1988, *BAICz*, **39**, 329.
- Hilditch, R.W., King, D.J., Hill, G., Poeckert, R. 1984, *MNRAS*, **208**, 135.
- Hilditch, R.W., King, D.J. 1988, *MNRAS*, **231**, 397.
- Hilditch, R.W., Collier Cameron, A., et al. 1997, *MNRAS*, **291**, 749.
- Jassur, D.M.Z., Khodadadi, A. 2006, *JApA*, **27**, 47.

- Kaluźny, J. 1983, *AcA*, **33**, 345.  
 Kaluźny, J. 1985, *AcA*, **35**, 327.  
 Kaluźny, J. 1986, *AcA*, **36**, 113.  
 Karimie, M.T., Duerbeck, H.W. 1985, *Ap&SS*, **117**, 375.  
 Kähler, H. 2004, *A&A*, **414**, 885.  
 Kreiner, J.M., Kim, Ch.-H., Nha, I.-S. 2001, *An Atlas of O-C Diagrams of Eclipsing Binary Stars*, Wydawnictwo Naukowe AP, Krakow.  
 Kreiner, J.M., Rucinski, S.M., Zola, S., Niarchos, P., et al. 2003, *A&A*, **412**, 465.  
 Kreiner, J.M. 2004, *AcA*, **54**, 207.  
 Kuiper, G. 1941, *ApJ*, **93**, 133.  
 Kurucz, R. 1993, *Atomic data for opacity calculations. Kurucz CD-ROM No. 1. - 18.*, Cambridge Mass. Smithsonian Astrophysical Observatory.  
 Leung, K.-Ch. 1974, *AJ*, **79**, 852.  
 Leung, K.-Ch., Wilson, R.E. 1977, *AJ*, **211**, 853.  
 Li, L., Han, Z., Zhang, F. 2004a, *MNRAS*, **351**, 137.  
 Li, L., Han, Z., Zhang, F. 2004b, *MNRAS*, **355**, 1383.  
 Li, L., Han, Z., Zhang, F. 2005, *MNRAS*, **360**, 272.  
 Lipari, S.L., Sisto, R.F. 1986, *MNRAS*, **220**, 883.  
 Lucy, L.B. 1967, *Zeitschrift für Astrophysik*, **65**, 89.  
 Lucy, L.B. 1968, *AJ*, **151**, 1123.  
 Lucy, L.B. 1973, *Ap&SS*, **22**, 381.  
 Lucy, L.B. 1976, *ApJ*, **205**, 208.  
 Lucy, L.B., Wilson, R.E. 1979, *ApJ*, **231**, 502.  
 Mauder, H., Kappelmann, N. 1982, *MitAG*, **55**, 72.  
 Milano, L., Russo, G., Terzan, A. 1987, *A&A*, **183**, 265.  
 Mochnacki, S.W. 1981, *ApJ*, **245**, 650.  
 Niarchos, P.G., Manimanis, V.N. 2003, *A&A*, **405**, 263.  
 Oh, K.-D., Ahn, Y.-S. 1992, *Ap&SS*, **187**, 261.  
 Paxton, B. 2005, *airXiv0405130*.  
 Pols, O., Tout, Ch.A., Eggleton, P.P., Han, Z. 1995, *MNRAS*, **274**, 964.  
 Pribulla, T., Rucinski, S.M. 2008, *MNRAS*, **386**, 377.  
 Pribulla, T., Rucinski, S.M., Blake R. M., et al. 2009, *AJ*, **137**, 3655.  
 Rahman, A. 2000, *PASP*, **112**, 123.  
 Rafert, J.B., Markworth, N.L., Michaels, E.J. 1985, *PASP*, **97**, 310.  
 Robertson, J.A., Eggleton, P.P. 1977, *MNRAS*, **179**, 359.  
 Rovithis, P., Rovithis-Livaniou, H., Suran, M.D., et al. 1999, *A&A*, **348**, 184.  
 Rucinski, S.M. 1969, *AcA*, **19**, 245.  
 Rucinski, S.M. 1986, *IAUS*, **118**, 159.  
 Rucinski, S.M. 1992, *AJ*, **104**, 1968.  
 Rucinski, S.M. 1999, *IAU Coll.170, ASPC*, **185**, 82.  
 Rucinski, S.M., Lu, W.-X., Mochnacki, S.W. 2000, *AJ*, **120**, 1133.  
 Rucinski, S.M. 2002, *AJ*, **124**, 1746.  
 Samec, R.G., Fuller, R.E., Kaitchuck, R.H. 1989, *AJ*, **97**, 1159.  
 Sarna, M.J., Fedorova, A.V. 1989, *A&A*, **208**, 111.  
 Siwak, M., Zola, S., Rucinski S. 2009, *airXiv0909.5415*, "Binaries - Key to Comprehension of the Universe" Brno, Czech Rep. 8-12 June 2009. To appear in Dec.2010 as ASP-CS435, eds. A. Prsa and M. Zejda.  
 Stefanik, R.P., Latham, D.W., Torres, G. 1999, *ASPC*, **185**, 354.  
 Stetson, P.B. 1987, *PASP*, **99**, 191.  
 Yakut, K., Eggleton, P.P. 2005, *ApJ*, **629**, 1055.  
 Van Hamme, W., Samec, R.G., Gothard, N.W., et al. 2001, *AJ*, **122**, 3436.  
 von Ziepel, H. 1924, *MNRAS*, **84**, 665.

- Webbink, R.F. 1976, *ApJS*, **32**, 583.  
Wilson, R.E. 1996, *Documentation of Eclipsing Binary Computer Model*.  
Zhu, L., Qian, S. 2006, *MNRAS*, **367**, 423.  
Zola, S. 1995, *A&A*, **294**, 525.  
Zola, S., Kreiner, J.M., Zakrzewski, B., et al. 2005, *AcA*, **55**, 389.  
Zola, S., Gazeas, K., Kreiner J.M., Zakrzewski, B. 2006, *Ap&SS*, **304**, 109.  
Zola, S., Gazeas, K., Kreiner, J.M., Ogłóza W., et al. 2010, *MNRAS*, **408**, 464.